Nuclear Instruments and Methods in Physics Research A265 (1988) 419–434
North-Holland, Amsterdam

RESULTS FROM A TEST OF A Pb–Cu LIQUID ARGON CALORIMETER

W. BRAUNSCHWEIG, J. TUTAS and E. VOGEL
I. Physikalisches Institut der RWTH Aachen, Aachen, FRG

M. WIDGOFF
Department of Physics, Brown University, Providence, USA

F.W. BRASSE, W. FLAUGER, J. GAYLER, V. KORBEL, J. MARKS and Ch. ZEITNITZ
Deutsches Elektronensynchrotron, DESY, Hamburg, FRG

S. BRINKMANN, K. RAUSCHNABEL and D. WEGENER
Physikalisches Institut der Universität Dortmund, Dortmund, FRG

E. BARRELET *, V. BRISSON, D. LELLOUCH **, P. PERRODO and C. VALLÉE
Ecole Polytechnique, Palaiseau, France

A.J. CAMPBELL
University of Glasgow, Glasgow, United Kingdom

H.T. BLUME +, K. LAU, F. LIPP and R. WEINSTEIN
Department of Physics, University of Houston, Houston, USA

H. GREIF, J. HUBER, C. KIESLING ++, D. LÜERS, H. OBERLACK and P. SCHACHT
Max-Planck-Institut für Physik und Astrophysik, München, FRG

E. VON GOELER and J. MOROMISATO
Department of Physics, Northeastern University, Boston, USA

B. DELCOURT and A. JACHOLKOWSKA
Laboratoire de l'Accélérateur Linéaire, Orsay, France

J. DUBOC and H. NGUYEN
Laboratoire de la Physique Nucléaire et Hautes Energies, Université de Paris, Paris, France

F. FERRAROTTO and B. STELLA
University of Rome and INFN, Rome, Italy

M. BESANÇON, G. COZZIKA, M. DAVID, J. FELTESSE, A. DE LESQUEN, P. VERRECCHIA and G. VILLET
Centre d'Études Nucléaires, Saclay, France

U. STRAUMANN
Physik-Institut der Universität Zürich, Zürich, Switzerland

Received 21 September 1987

Results from a test with a lead–copper calorimeter in liquid argon are presented. The electromagnetic energy resolution obtained is $10\%/\sqrt{E}$. For hadronic showers the software weighting technique is demonstrated to work. A hadronic energy resolution of $50\%/\sqrt{E}$ is found.

1. Introduction

In order to measure the energy of single particles and jets, the forthcoming H1 experiment [1] at HERA relies heavily on liquid argon (LAr) calorimetry. The energy and angles of electrons and photons will be measured in a first section with lead absorbers whereas the more penetrating hadrons are also recorded in a second section with stainless steel absorbers.

Here we report on a test experiment with the main goal to demonstrate that a noncompensating lead/copper calorimeter performs as anticipated [1], in particular to verify that the energy resolution can be improved by corrections of π^0 fluctuations. This is expected by Monte Carlo studies [2] and has been shown in previous experiments for other types of calorimeters [3,4].

The experimental setup is described in section 2. Section 3 gives results on the performance of the calorimeter for incident electrons (section 3.2) and pions (sections 3.3). We discuss only hadron showers which are fully contained in the LAr calorimeter. A more detailed report [5] containing also results for showers penetrating in a gas tail catcher is in preparation.

2. Experimental setup

2.1. Introduction

Using a CERN SPS beam, a series of run periods between June and November 1986 was dedicated to test essentially two different versions of calorimeter configurations. A hadronic copper stack was common to both versions. In the first four run periods, a conventional electromagnetic (e.m.) stack and an additional stack using iron as tail catcher were installed inside the LAr (version A). In the last run period, these stacks were replaced by an e.m. stack exploiting the technique of high resistive coating and a tail catcher which operated with plastic streamer tubes outside of the LAr (version B). An overview of the basic parameters is given in table 1. All stacks operating in LAr were housed in a cryostat. Fig. 1 sketches the layout of the experiment.

2.2. The beam and its detectors

2.2.1. The beam

The calorimeter was installed in the H6 beam [6] of the North Hall 1 at the CERN SPS. The beam optics is summarized in fig. 2. This beam provided electrons, muons, pions, protons, and kaons in the momentum range $5 \leq p \leq 250$ GeV/c. Most of the data were taken with electrons or pions. The beam was run in two modes:

(a) *Secondary mode ($p \geq 100$ GeV/c).* In this mode, the beam was run with the primary target only. Electrons and pions were separated spatially by synchrotron

Table 1
Basic parameters

		Version A	Version B
E.m. stack (EC)	material	Pb/LAr	Pb/LAr
	total length	22.8 X_0, 1.1λ	26.2 X_0, 1.1λ
Hadronic stack (HC)	material	Cu/LAr	Cu/LAr
	total length	6.12λ	6.12λ
Tail catcher (TC)	material	Fe/LAr	Fe/plastic streamer tubes
	total length	2.88λ	4.57λ

* Now at Université de Paris, France.
** Now at Weizmann Institute of Science, Israel.
+ Now at Max-Planck-Institut für Physik und Astrophysik, München, FRG.
++ Heisenberg-Stipendiat der Deutschen Forschungsgemeinschaft.

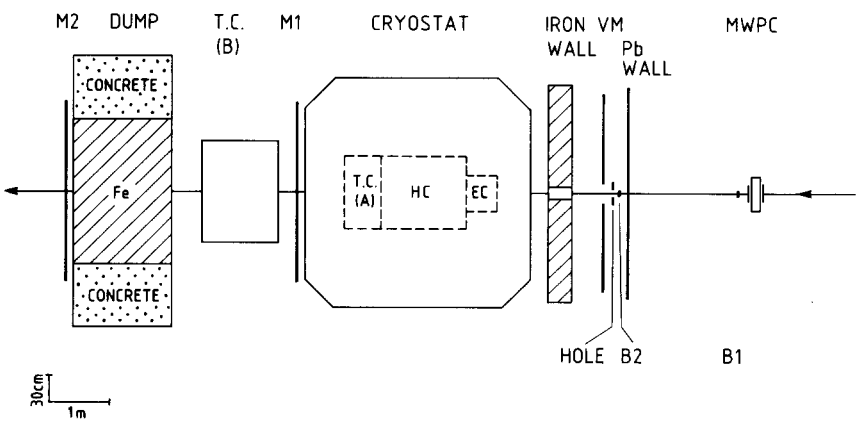

Fig. 1. Schematic view of the test setup. The main elements are: electromagnetic calorimeter section (EC), hadronic calorimeter section (HC), tail catcher setup A/B (TC).

radiation [7]. The typical loss of energy for electrons occurs mainly in BM3 and is for example about 2% at 120 GeV. When the beam after BM3 is tuned for electrons, the two profiles are easily separable at the collimator C3. The momentum spread was typically $\Delta p/p = 0.8\%$ for e and $\Delta p/p = 0.05\%$ for π.

(b) *Tertiary mode [8] ($p \leq 100$ GeV/c).* A secondary target (aluminum or polyethylene) was installed just after the collimator C3. The first part of the beam (between the two targets) was tuned for the highest possible energy (150–250 GeV), the second part for the requested low momentum. The tertiary particles (e or π) were tagged by two Cherenkov counters with ring selection (CEDARs [9]) in the momentum range $10 \leq p \leq 80$ GeV. The momentum spread was typically $\Delta p/p = 0.8\%$.

2.2.2. The beam detectors

Two multiwire proportional chambers (MWPCs) were installed in front of the calorimeter. Each has an active region of 25×25 cm^2 and consists of a horizontal and vertical anode plane, with a distance between the two chambers of 19 cm and a position resolution of 2 mm (FWHM). The chambers were used to monitor the beam geometry during tuning and to select events with only one hit per plane in the data analysis, removing therefore showers originating from the material located upstream in the beam (0.44 radiation lengths (X_0)).

2.2.3. The trigger detectors

The beam particles were defined by the two CEDARs, the two MWPCs, and two scintillation counters (B_1 and B_2) with lateral dimensions of 3×3 cm^2. Beam halo particles were detected by a set of three scintillator walls: one in front of the calorimeter (veto wall, VM), a second one behind the cryostat (M1), and a third wall (M2) behind the 1.6 m long beamdump of iron (see fig. 1). Each wall consisted of 10 scintillation counters, each 120 cm long and 20 cm wide, overlapping by about 5 mm and oriented vertically. The front part of the first wall was additionally covered with about $2X_0$ of lead to improve the sensitivity for low energetic photons. Furthermore, the veto wall was shielded against backscattering of particles from the calorimeter by an iron wall of 40 cm thickness. Holes in the lead (diameter 4.2 cm) as well as in the scintillator wall (diameter 2.0 cm) defined the aperture of the beam.

2.3. The liquid argon system

2.3.1. The electromagnetic calorimeter (EC)

The relevant parameters of the two types of lead stacks of the calorimeter version A ($22.6X_0$) and B ($26.2X_0$) respectively are summarized in table 2a. The total number of electronic channels in the EC is 240.

Version A: One cell unit of the e.m. calorimeter version A is shown in fig. 3a. The readout boards (ROB) were positioned in the center of the LAr gap by 20 teflon spacers of 1.5 mm thickness. The positioning of the absorber plates and readout boards was done by 4 rods with teflon washers (1.5 mm thickness). The ROBs were made out of two double-sided FR4 boards glued together, with copper pads of 35 μm thickness on both sides and readout lines in the middle. The pads are separated by 1 mm. The pad structure with the readout lines (0.3 mm) of one quadrant of the boards is shown in fig. 4. A 5-fold longitudinal segmentation has been chosen with 8, 8, 8, 8, and 32 ROBs connected longitudinally together. Each of these longitudinal sections has 48 towers connected to charge sensitive preamplifiers. The capacitance of the individual towers (including cables) varied between 0.8 and 1.5 nF for the first four sections and between 1.8 and 4.6 nF for the fifth one. The total gap capacitances of the sections were measured to be 60 nF for each of the first four segments and 163 nF for the fifth.

The high voltage (hv) is applied via five separate lines to the lead plates of the longitudinal segments. The high voltage blocking capacitors (80, 195, 211, 178, and 221 nF) are connected to ground next to each section. Additional blocking capacitors (2000 nF per line) outside of the cryostat were added. With these blocking capacitances the total negative crosstalk (section 3.1.2.) was kept below 15%.

Version B: The main difference compared to config-

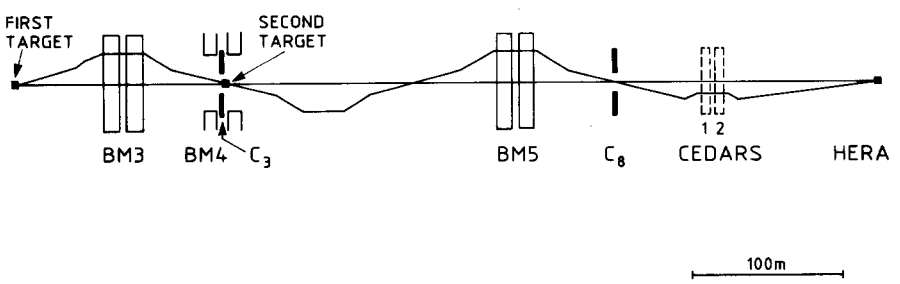

Fig. 2. Schematic of the optics of the H6 beam.

Table 2a
Parameters of the two types of lead stacks

	Version A	Version B
Lead plate (mm^3)	$1.86 \times 420 \times 420$	$2.4 \times 420 \times 420$
LAr gap (mm)	2×1.5	2.8
ROB thickness (mm)	1.12	0.8
ROB position	central in gap	on lead plate
Number of ROBs	64	57
Molière radius (cm)	3.7	3.3
Length [mm/X_0/λ]	376.0/22.8/1.06	377.5/26.2/1.13
Long segmentation	$2.85/2.85/2.85/11.4 X_0$	$2.7/3.6/3.6/3.6/12.6 X_0$
High voltage	on lead	on high resistive foil

Table 2b
Parameters of the copper stack

Copper plate (mm^3)	$5 \times 820 \times 800$
LAr gap (mm)	2×1.5
Number of ROBs	154
Length [mm/λ]	1391/6.12

uration A is: The high voltage was applied via a high resistive foil glued either onto the ROB or onto the absorber plate. In order to minimize the variation of the high voltage over the area of the high-resistive-coated (HRC) plane, a line of conducting silver paint was applied along one side of the foil. All lead plates of the stack were connected in parallel to ground. Thus, a blocking capacitance of typically 50 nF per plate was achieved and, therefore, no blocking capacitors were needed.

The calorimeter consists of two parts differing in cell structure. The structure of the first 15 cells of the calorimeter version B is shown in fig. 3b. For HRC a Kapton foil (75 μm) is glued to every other lead plate, and a mixture of epoxy glue and conducting soot (40 μm layer) has been sieve-printed onto this foil. The resistance of the HRC varies from foil to foil between 100 and 70 MΩ/square. A lead plate with a ROB glued on each side is placed between the two lead plates with the HRC. The ROB is a two-layer board (0.8 mm thick) with the readout lines on the inner side. A Kapton foil (75 μm) was glued between ROB and absorber. The LAr gap was defined by teflon spacers. The averaged gap thickness was 2.78 mm with a maximum variation of 0.35 mm. These first 15 cells were divided longitudinally into four sections consisting of 3, 4, 4, and 4 cells with 48 towers per section. The cell structure of the back part of the calorimeter is shown in fig. 3c. In contrast to the front part, the HRC was glued to the ROBs. All 14 cells were longitudinally grouped in one section. The total gap capacitances of the sections were measured to be 73, 91, 90, 89 and 343 nF. The HRCs of each longitudinal section were connected in parallel to one high voltage channel. In this scheme, a large blocking capacitance was achieved, and the preamplifiers were protected against possible hv breakdowns in the LAr gap. Thus, the number of dead channels was kept well below 1%.

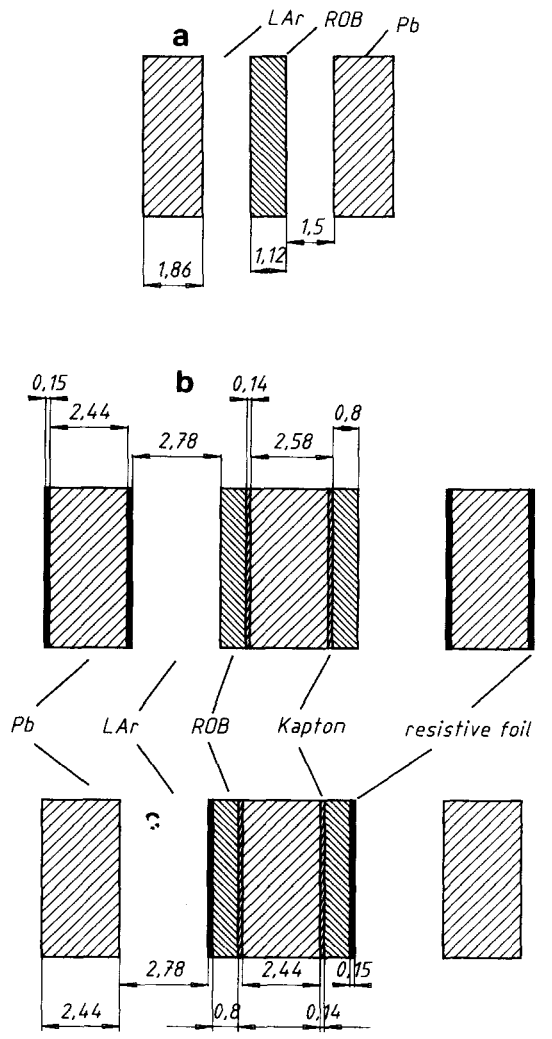

Fig. 3. Cell structure of both EC versions: (a) version A, (b) version B (front part), (c) version B (back part).

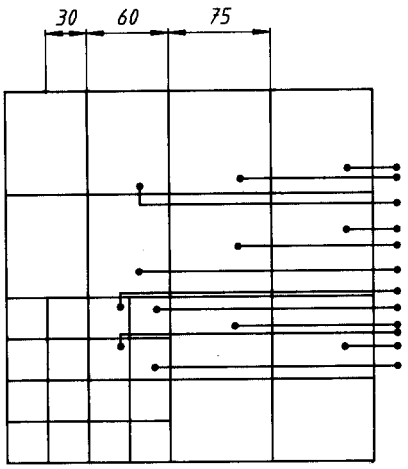

Fig. 4. Pad structure and readout lines of one quadrant of the EC ROB.

2.3.2. The hadronic calorimeter (HC)

The hadronic section of the calorimeter (see table 2b) consisted of two sections, the first one with 6.12 interaction lengths (λ) of copper and the second one (version A only) with 2.88λ of iron. This latter section has been used to study the leakage of the showers (tail catcher) and was removed when the gaseous tail catcher was installed behind the cryostat. The basic cell structures are shown in fig. 5a (copper section) and 5b (iron section).

Each cell consisted of an 820×800 mm^2 absorber plate followed by a LAr gap, a G10 ROB, a second LAr gap and the next absorber plate. In the copper section, the plates were 5 mm thick with measured tolerances of the flatness of 0.4 mm and of the thickness of 0.05 mm. The argon gap was 1.5 mm wide and maintained by plastic spacers located 80 mm apart on either side of the ROB. In the iron section, the absorber plates were 25 mm thick with tolerances less than 0.1 mm on thickness and flatness. The argon gap was 4 mm thick, maintained in the same way as in the copper section. The ROBs were made of 1 mm thick G10 plates cladded with 35 μm thick copper. They acted as charge collecting electrodes. These boards were etched on both sides to form a strip pattern as shown in fig. 5c. In consecutive cells, the ROBs were mounted with the strip orientation alternating between vertical and horizontal. Each strip of a given orientation was ganged to the corresponding ones of the following ROBs with the same strip orientation, thus defining longitudinally segmented towers (fig. 6). In this way, two interleaved cell structures were provided for each longitudinal segment. Such a configuration allows to study the effect of sampling fluctuations. In total, the copper section was subdivided into 6 longitudinal segments with 26 elementary cells each, except for the last one which had 24 cells. The iron section was subdivided into 2 longitudinal segments with 9 cells per segment (fig. 6).

Each segment has 40 electronic channels (20 vertical and 20 horizontal). This leads to a total of 320 channels for setup A and 240 channels for setup B.

The high voltage was applied to the absorber plates in an interleaved way to reduce the dead volume in case of a short circuit in one of the gaps. The 175 planes of setup A were connected to the high voltage via 28 separate lines. The blocking capacitors varies between 200 and 600 nF.

The EC calorimeter was mounted onto the same frame as the HC, just in front of the first copper plate of the HC. This whole assembly was mounted on rollers for moving into the cryostat.

2.3.3. Cryostat and cryogenics

The cryostat is of the horizontal type and has a

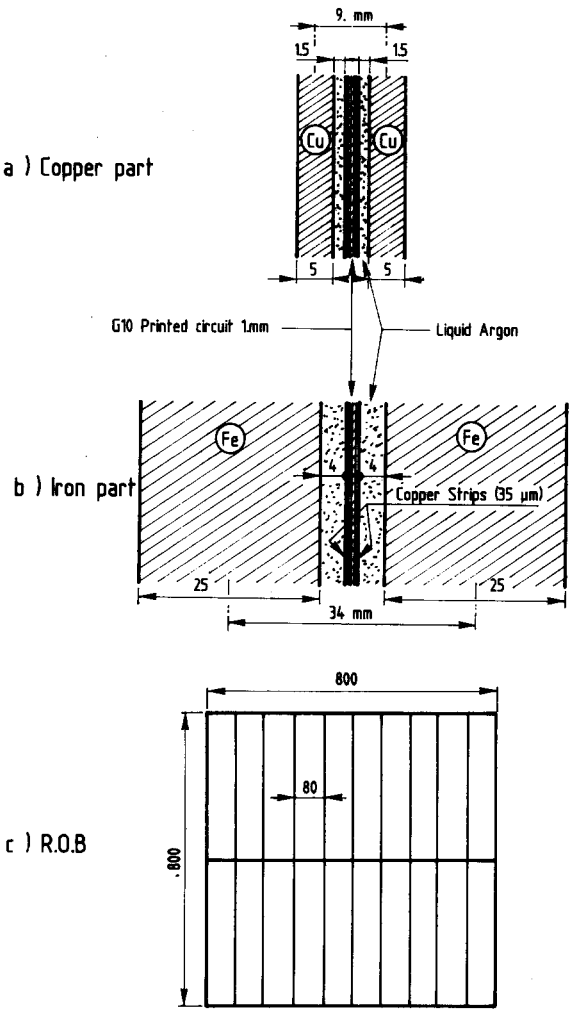

Fig. 5. Basic cell of the hadronic calorimeter: (a) copper section, (b) iron section, (c) strip pattern.

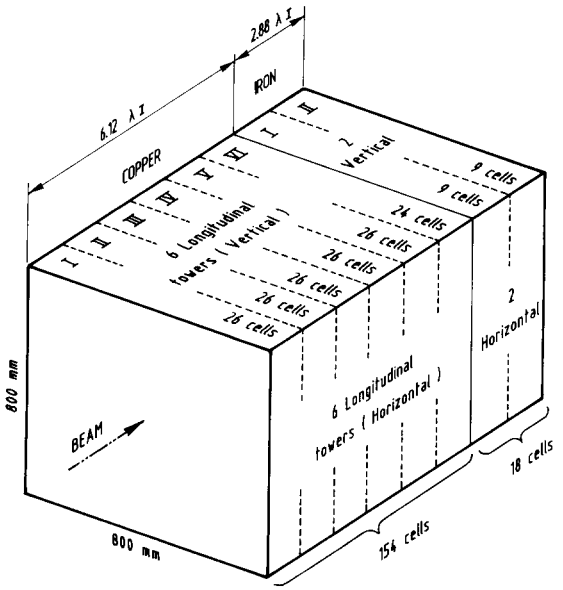

Fig. 6. Longitudinal segmentation of the hadronic calorimeter.

removable front end for loading the calorimeter. The carriage on which both the e.m. and the hadronic calorimeters are mounted can roll on rails fixed to the inner wall of the cryostat. The beam particles enter the cryostat through a 550 mm long vacuum tube of 100 mm diameter with thin window at both ends. The useful diameter of the vessel is 1800 mm and the overall length 3000 mm. The capacity of this cryostat is about 6 m^3 of liquid argon. Insulation against heat losses is provided by a layer of polyurethane foam 400 mm thick.

Refrigeration is provided by liquid nitrogen circulation in a heat exchanger located in the vapour phase of the argon. Total cooldown time to reach LAr temperature was about three days. In stable operation, the absolute pressure in the vapour phase of the argon was maintained at 1.2 bar, by regulating the liquid nitrogen flow in the heat exchanger. Warming up after emptying the cryostat took about five days. This was achieved by using a 1600 W heater located at the bottom of the vessel.

Nine ports on the top of the cryostat serve as feedthroughs of cryogenic and pumping lines, signal and hv cables, as well as cables connected to the sensors monitoring the pressure and temperature at various locations within the vessel.

The purity of the argon in the cryostat was monitored continuously throughout the experiment by sampling gas taken from the vapour phase of the argon. The O_2 contamination was of the order of 2 ppm except during the September/October run periods (data of setup A) when it was of about 22 ppm.

2.3.4. *Electronics*

The electronics chain for the treatment of the LAr pulses is shown in fig. 7. A total number of 560 channels was employed. Each channel consisted of five modules: charge sensitive preamplifier, line driver, differential amplifier, shaper, and ADC. The preamplifiers were located as close as possible to the feedthrough of the signal cables (97 Ω) out of the cryostat. The cable length from the LAr cells to the preamplifiers was 9 m. The line driver differentiated the signal and transmitted it over a distance of 60 m to the differential amplifier and shaper. The shaping time was 2 μs. The signal was digitized by a charge sensitive ADC of the type LCR 2280. The gate for the ADC was set to 500 ns.

The intrinsic noise of the preamplifier depends on the capacitive load. The incoherent noise in an entire channel was found to be $Q_T[e_0] = 11000 + 4400 C_D[\mathrm{nF}]$ where C_D is the detector capacitance, which was in the range of 0.3–9 nF. By summing over all electronic channels, we found a coherent contribution (pickup) to the total noise of 50–80% under beam conditions.

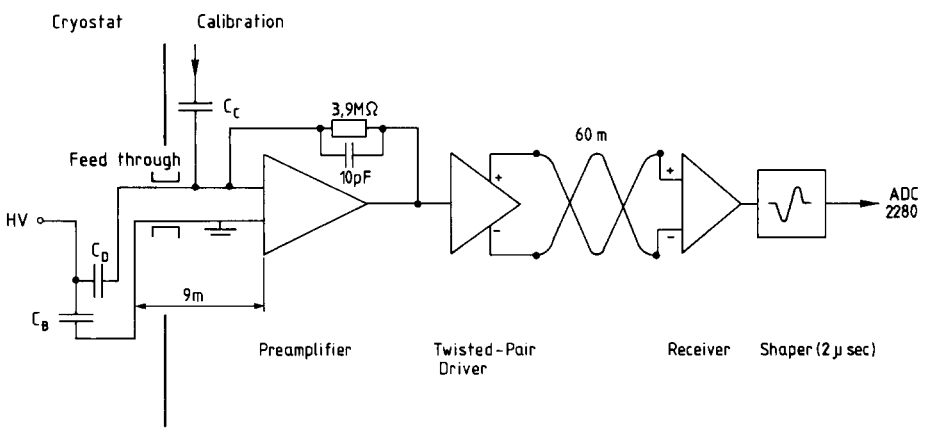

Fig. 7. Electronic chain.

The electronics chain was calibrated by feeding a voltage pulse via a 10 pF capacitor into each preamplifier. This capacitor was located on the preamplifier card and had a precision of 1%. This charge input could be attenuated by a computer-controlled switch. Thereby, the whole dynamic range of the electronics was scanned in fine steps. The method guaranteed to find the exact pedestal values as well as the precise ADC channel to charge conversion for each channel, and to determine the crosstalk by pulsing simultaneously only non-adjacent channels. The calibration was repeated once per day. Over a period of 30 d the stability of the pedestals was around 1σ of the pedestal distribution, and the slopes did not change by more than 0.5%.

2.4. The gas tail catcher

The tail catcher calorimeter used iron as absorber and wire chambers as active detector elements. The chambers were operated in the limited streamer mode with the readout being performed by strips (digital) and pads (analog).

The detector consisted of 20 iron plates with lateral dimensions 110×125 cm^2, and with thicknesses of 2.5 and 5.0 cm. The measurements described in this paper were performed with a sampling thickness of 7.5 cm ($4.26 X_0$, 0.44λ). The total thickness, including the active detector planes, amounted to 4.57λ. The inactive material between the HC and the front plate of the tail catcher corresponded to 1.4λ. A detailed description of this calorimeter and its performance will given in forthcoming papers [5,10].

2.5. Trigger and data acquisition

The trigger scheme for the test setup was laid out to provide basically two features:

- Identify the beam particle generating the trigger and in addition allow for some special purpose triggers.
- Ensure that for a triggered event only one particle enters the calorimeter.

Taking into account the setting of the two CEDARs, separate triggers were available for electrons and/or pions. From the eight individual signals provided by each CEDAR, six were demanded to be in coincidence with B_1 and B_2 for triggering the event. The more restrictive options with higher coincidence level were latched for off-line selection. For momenta $p \geq 100$ GeV/c electrons and pions were selected by synchrotron radiation as described above. Muons were identified by the scintillation wall behind the beam dump. For permanent pedestal monitoring events were randomly triggered during the burst time without any particle crossing the detector.

In order to avoid more than one particle entering the calorimeter within the sensitive time – given by the

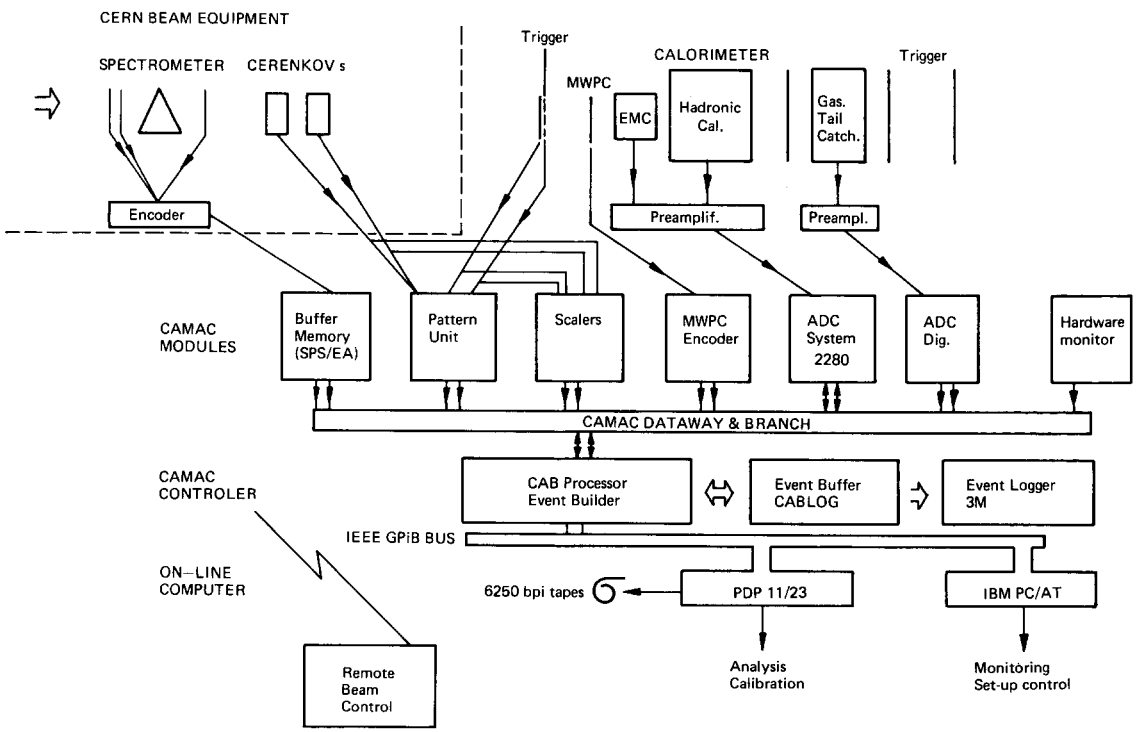

Fig. 8. Schematic diagram of the data acquisition system.

rather long charge collection time in the LAr gap – events were accepted only if there was no second beam particle within 10 μs before and 3 μs after the event.

Two computers have been used for the data acquisition, an IBM PC AT2 and a PDP 11-73, both boosted by a fast processor CAB [11], as shown in fig. 8. The IBM PC drove the CAB programs and monitored the whole set up and the data acquisition. The CAB processor read the detector components in 2 ms and used another 2 ms for histograms and additional computations. Furthermore, if offered the possibility to filter the data on-line. Between bursts, the event buffer was dumped on a 3M cartridge (as an alternative for data recording) and to the PDP. The PDP 11-73 drove a 6250 BPI magnetic tape and had three functions: (a) writing the events onto tape: (b) histogramming for fast on-line analysis; (c) monitoring and recording the calibration and calorimeter data in a stand-alone mode. With an event buffer size of 1.2–2 kbytes the typical data rate was 200 events per 2 s burst when writing on tape.

3. Performance and results

3.1. Data corrections

3.1.1. High voltage plateau curve

Fig. 9 shows the dependence of the average deposited charge in EC or HC, on the electric field applied for electrons and pions, normalized to the response at the highest electric field. For the EC as well as for the HC of the setup B, a plateau value of about 1 kV/mm was obtained. In contrast, the data of setup A suffered from a serious oxygen contamination in the LAr and therefore, a plateau could not be reached. This, however, did not influence the energy resolution for setup A.

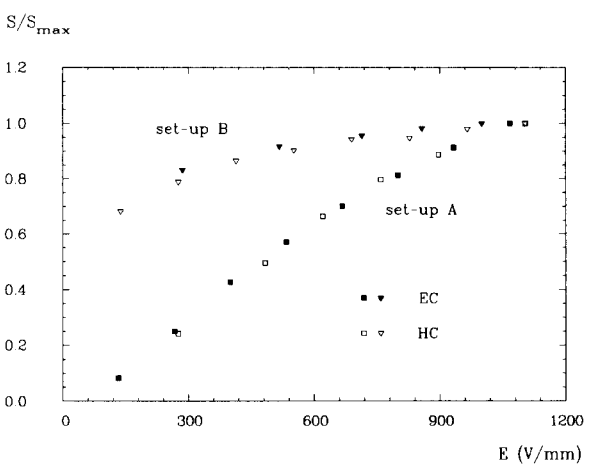

Fig. 9. High voltage plateau curve for EC and HC (setup A and B).

3.1.2. Crosstalk

The data had to be corrected for the following effects:

(a) *Negative crosstalk*. The pads hit by a shower receive a positive signal, but the neighbouring pads a negative one. This is due to the fact that for the transient state, the lead plates are effectively isolated from the high voltage. Thus, a positive charge in the center induces a negative one in the neighbouring region. These two charges are proportional to the ratio of pad capacitance to blocking capacitance and, therefore, can be systematically corrected. The maximum correction applied for any longitudinal section of EC or HC was 15%.

(b) *Positive crosstalk*. For the EC version B, we observe, on the contrary, too much energy in the peripheral pads due to an insufficient grounding of the lead plates for higher frequencies. This has been corrected by studying the correlation between each channel and the total energy deposited by pions. This yields corrections per channel in the range 0.04–0.6% of the total energy in the EC. Varying these corrections within the uncertainties has no influence on the resolution of hadron showers.

3.2. Results for incident electrons

Besides the beam trigger condition (see section 2.5) the data selection criteria were:
- no hit in the veto-wall,
- just one cluster in each of the four MWPC planes.

As an example, fig. 10 shows the distribution of the total deposited charge in the central pads (16 per longitudinal section) of the EC for electrons of 166 GeV for setup B. The mean value and the width of these distributions were obtained from a Gaussian fit to the data. The small low energy tail is mainly due to bremsstrah-

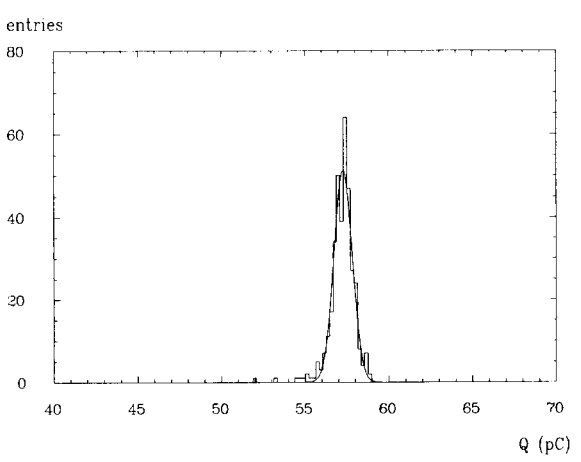

Fig. 10. 166 GeV e: charge distribution for the sum over all central pads for the EC of setup B.

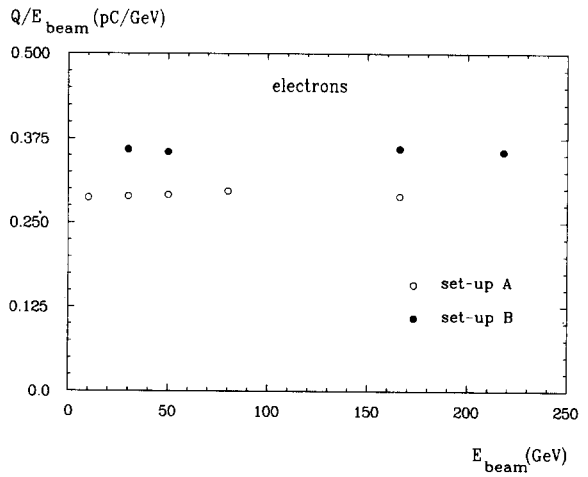

Fig. 11. Measured normalized charge for the EC of setup A and B as a function of the beam energy.

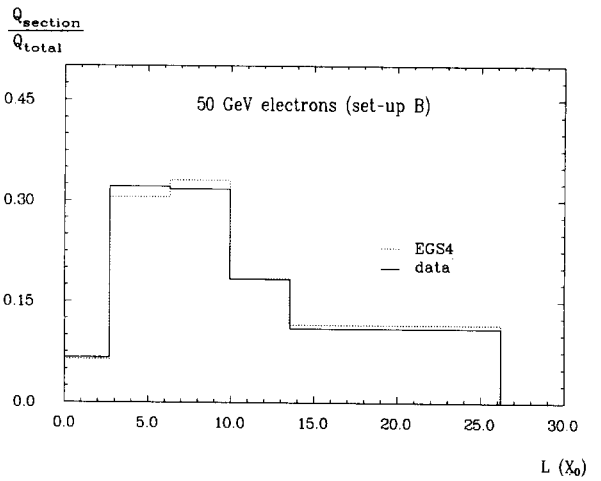

Fig. 12. Longitudinal shower profile for electrons of 50 GeV (setup B).

lung of electrons upstream in the beam line. The energy dependence of the total deposited charge per energy for the two configurations of the e.m. calorimeter is shown in fig. 11. At 166 and 218 GeV, the energy deposited in the first longitudinal section of the HC has been included (about 1% of the total energy deposit). The energy response is linear over the full energy range from 10 to 218 GeV, the maximum deviation being 1.5%. For setup A, the measured charge was lower due to some oxygen contamination of the LAr (see section 2.3.3). From Monte Carlo (MC, EGS4) [12] calculation the ratio of charge to energy deposit for incident electrons is expected to be 0.338 pC/GeV for setup B. This agrees with the measured value of 0.357 pC/GeV within the uncertainty of the absolute charge prediction from MC. The longitudinal shower profile for 50 GeV incident energy is shown in fig. 12 and compared with the Monte Carlo (EGS4) prediction. Here the material in front of the e.m. calorimeter ($1.3X_0$ and $1.1X_0$ for setup A and B respectively) has been included and good agreement is found. Figs. 13a and b show the dependence of the energy resolution σ/E on the energy E as obtained from the energy deposited in the central pads (16 per longitudinal section) for the two versions of the e.m. calorimeter. This energy dependence can be parametrized as

$$\sigma/E = \sqrt{a^2/E + b^2/E^2 + c^2},$$

where a represents the sampling fluctuations, b the contribution due to electronic noise as determined from randomly triggered events and c the momentum resolution of the beam and intercalibration errors. For setup A (B) the parameters a and c (a) have been determined from a fit, and the parameter b has been

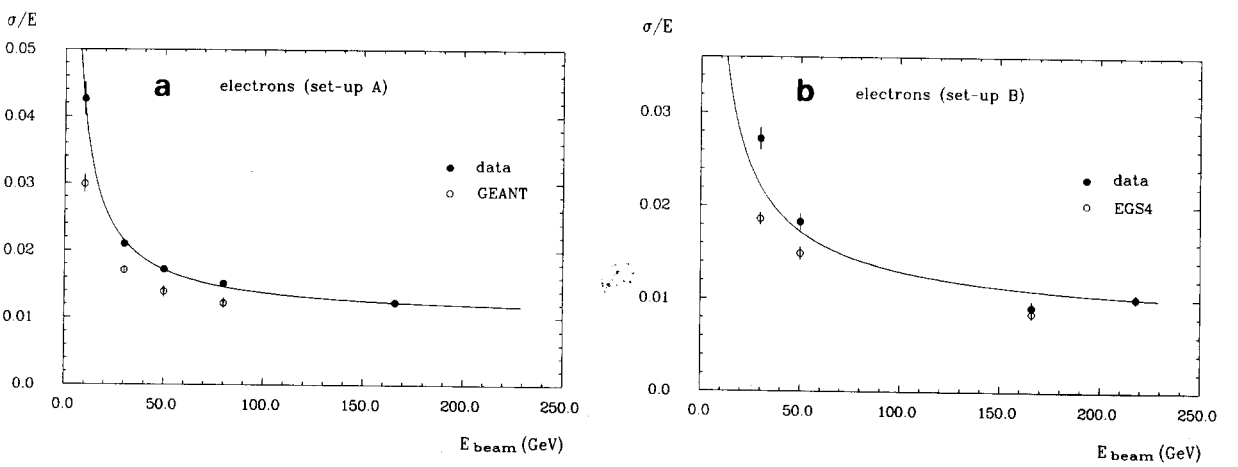

Fig. 13. Energy resolution for a sum over all central pads ((a) for setup A, (b) for setup B). In the MC values effects due to noise and beam width are not taken into account.

Table 3
Comparison of the energy resolution for electrons with the MC prediction

	a [$\sqrt{\text{GeV}}$]	b [GeV]	c	a [$\sqrt{\text{GeV}}$] (EGS4/GEANT)
Version A	0.090 ± 0.004	0.286	0.010 ± 0.005	0.096 ± 0.003
Version B	0.112 ± 0.003	0.250	0.007	0.104 ± 0.003

determined from randomly triggered events. In addition, for setup B, the parameter c has been fixed to $c = 0.007$. The open circles in fig. 13a and b are the values predicted from MC (GEANT [13] and EGS4 [12] respectively) neglecting contributions due to noise and beam momentum resolution. The solid line represents the parametrization as described above. Tables 3 and 4 summarize the results, the errors are statistical ones only. The MC results are compatible with the parameter a obtained from the data. Instead of adding the energy deposited only in the central pads, also the total energy deposit was studied. Here, for noise suppression, a threshold cut of 3σ of the pedestal distributions has been applied. The resolutions thus obtained are compatible with the results given above.

3.3. Results for pions

The results presented are mainly from setup B with pion energies of 30, 50, 170, and 230 GeV. Some results will also be given for setup A.

3.3.1. Event selection

For all energies besides the beam trigger condition (see section 2.5) at least one of the two Cherenkov counters was required. This was also true at 170 and 230 GeV where the electrons were identified by synchrotron radiation. Further selection criteria were:
- no hit in the veto wall;
- in each of the four MWPC planes just one cluster.

Events were accepted for further analysis only if none of the digital strips of the gas tail catcher (section 2.4) fired. This corresponds to a rejection of events which deposit more than about 2 GeV in the tail catcher. The veto implies that the showers are nearly fully contained within 8.6λ of which the first 7.2λ (section 2.3) are used to measure the shower energy. The fraction of events removed by the veto is given in table 5. At most 1.3% of the events are nevertheless not fully contained due to lateral leakage before the TC and were thus not vetoed. The energy measurement by the tail catcher will be discussed elsewhere [10]. For the data of setup A, a similar cut of about 2 GeV in the liquid argon tail catcher was used.

Table 4
Energy resolution for electrons

Beam energy [GeV]	σ/E [%]
Version A	
10	3.56 ± 0.25
30	1.89 ± 0.06
50	1.63 ± 0.05
80	1.48 ± 0.04
166	1.22 ± 0.03
Version B	
30	2.73 ± 0.12
50	1.86 ± 0.08
166	0.91 ± 0.07
218	1.01 ± 0.05

3.3.2. Corrections and noise reduction

The data were corrected for crosstalk effects as described in section 3.1. The electronic noise when summing up all channels amounted to typically 1 GeV in the EC and 2 GeV in the HC. This influenced the energy resolution mainly at the lowest pion energy of 30 GeV. To reduce the noise contribution the following procedure was applied: Individual channel signals were only accepted if the measured charge was above a given threshold or if at least one of the directly neighbouring channels (in x or y or z direction) was above that threshold. These thresholds were taken to be 50 MeV for sections 1 to 4 of the EC, 100 MeV for section 5 of the EC, and 150 MeV for the HC. This corresponds roughly to 3σ of the pedestal distributions and also to about the energy deposit of one minimum ionizing particle.

With these cuts applied to the pions of 30 GeV, the noise contribution was reduced to 0.3 GeV and to 0.8 GeV in the HC. Although at higher energies the noise contribution was much less severe, the analysis procedure was kept the same.

3.3.3. Energy calibration without π^0 weighting

Each channel was calibrated for the charge deposited as outlined in section 2.3.4. The relation to deposited energy was established by comparison with the various

Table 5
Fraction of events vetoed by the tail catcher

E [GeV]	30	50	170	230
Fraction	0.11	0.20	0.51	0.52

Table 6
Calibration constant, resolution and effective e/π ratio for pions (without π^0 weighting technique)

E [GeV]	30	50	170	230
c_E [GeV/pC]	3.26	3.11	3.00	2.96
c_H [GeV/pC]	4.38	4.30	4.10	4.18
σ/E	0.111	0.090	0.057	0.050
$\sigma/\sqrt{E}$	0.61	0.64	0.74	0.76
Effective e/π	1.17	1.13	1.09	1.07

beam energies. The total deposited energy by an incident pion is calculated according to

$$E = c_E Q_E + c_H Q_H,$$

where Q_E and Q_H are the total charges measured in EC and HC respectively. The two calibration constants c_E and c_H, which depend on the sampling ratio and absorber material, were determined for each beam energy by the two conditions:

(a) $\langle E \rangle = E_{beam}$,

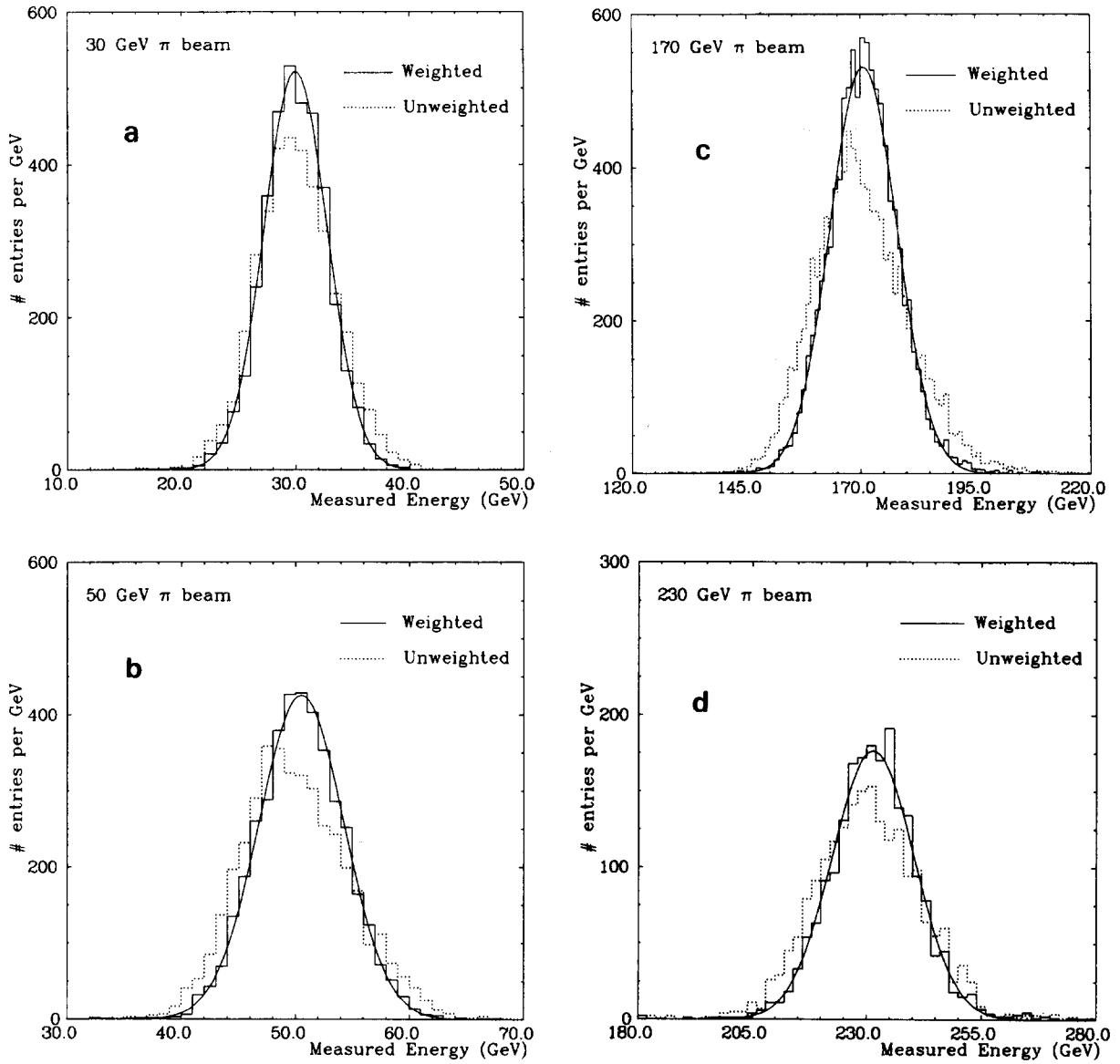

Fig. 14. Energy distributions for pions of 30 (a), 50 (b), 170 (c), and 230 (d). GeV. The dotted histogram shows the unweighted distribution, the solid histogram the corresponding distribution using the weighting technique. The solid lines represents a Gaussian fit to the weighted distribution.

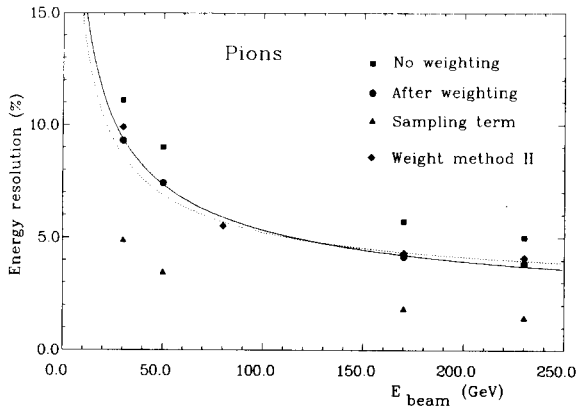

Fig. 15. $\sigma/\langle E\rangle$ vs pion energy. Shown are the results without and with weighting for the data of setup B and with the weighting method 2 for the data of setup A. The solid (dotted) line represents a fit using $\sigma/\langle E\rangle = \sqrt{A^2/E + B^2}$ to the data of setup B (A). In addition, the pure sampling term contributions are shown as well.

(b) the width of the energy distribution is minimum.

The resulting calibration constants are given in table 6. They decrease slowly with energy as expected if the signal for electrons is larger than for pions, since the electromagnetic fraction of the hadronic shower increases with energy. Using c_E and c_H as defined above for pions, a direct comparison of the mean measured energies for pions and electrons of the same energy leads to effective e/π ratios as given in table 6. These e/π ratios are effective values for the present EC (1λ) and depend on the calibration procedure to determine c_E and c_H.

The energy distributions obtained are shown in fig. 14 (dotted line). The resolution $\sigma/\langle E\rangle$, as obtained from a Gaussian fit to the energy distribution, decreases with increasing energy, but slower than $1/\sqrt{E}$ (see table 6 and fig. 15).

3.3.4. π^0 weighting

The fluctuations of the π^0 content of hadronic showers deteriorate the energy resolution as the calorimeter response is different for electromagnetic and hadronic energy. Local high energy concentrations in the shower development are mainly due to π^0's and increase the total measured energy of an event since $e/\pi > 1$. This is demonstrated in fig 16a showing the total measured energy (calibration as in section 3.3.3) versus the maximum local single channel energy per event in the HC in the case of incident pions punching through the EC. Comparable plots have been shown before for different calorimeters (e.g. refs. [3,4]). Similarly, the measured total energy is large for showers, where most of the energy is absorbed in the EC (fig. 17a). The measured energy of this kind of hadronic showers compares well to the energy of electron initiated showers. The method chosen to correct for the π^0 fluctuations is motivated by the approach of rf. [3] (for a somewhat different algorithm see below). For each event "weighted energies" are defined for the EC and the HC by

$$E_E^w = \sum_{EC} [E_i(1-\eta_E E_i)], \quad \text{with} \quad (1-\eta_E E_i) \geq C_E^{min},$$

$$E_H^w = \sum_{HC} [E_i(1-\eta_H E_i)], \quad \text{with} \quad (1-\eta_H E_i) \geq C_H^{min},$$

where E_i are the energies of the individual channels calibrated as outlined in section 3.3.3. and the corrections $(1-\eta E_i)$ are limited to C_E^{min} and C_H^{min} respectively. At a given energy the parameter η_H is taken the

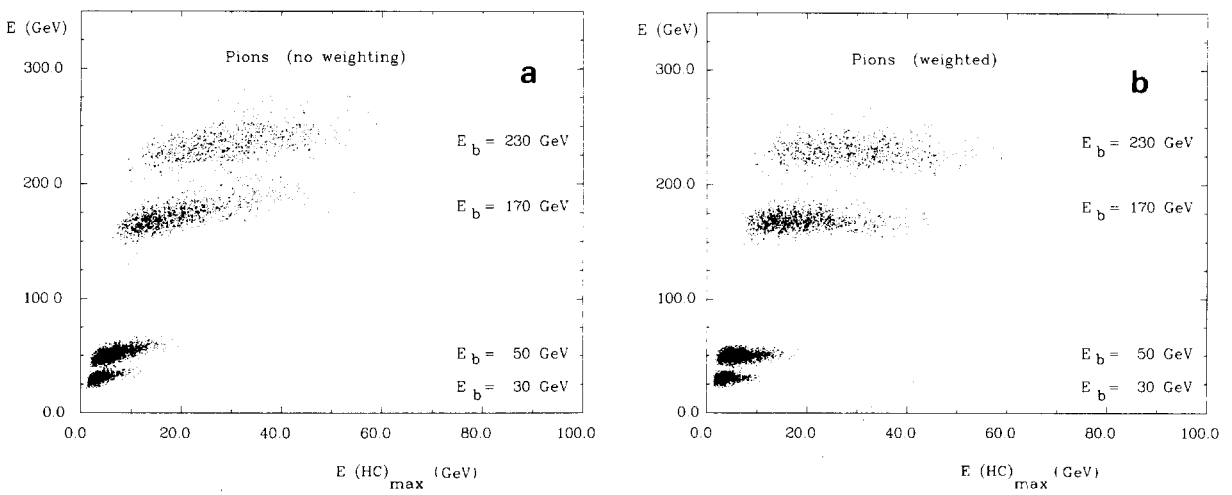

Fig. 16. Scatter plot of E vs the maximum single channel energy E_{max} in HC, for pions of 30, 50, 170, and 230 GeV: (a) no weighting, (b) weighting.

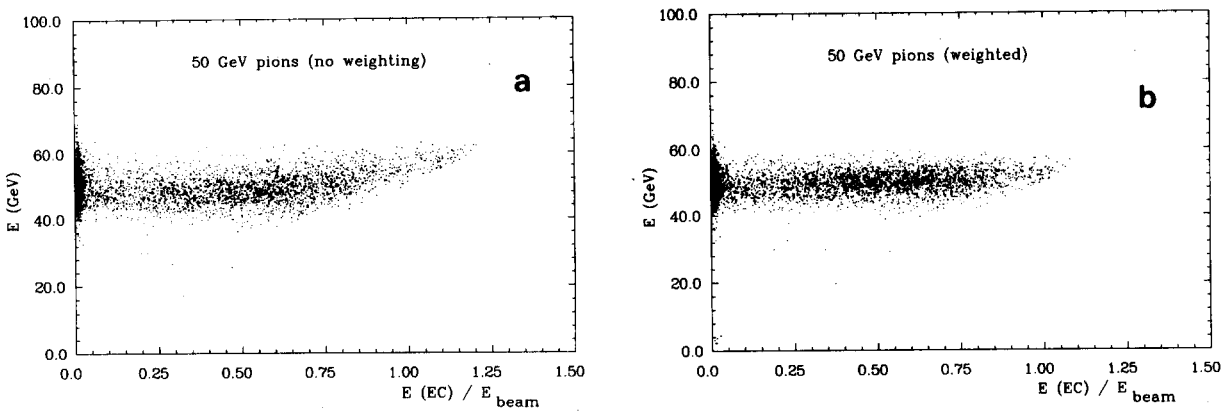

Fig. 17. Scatter plot of E vs E_{EC}/E_{beam} for pions of 50 GeV: (a) no weighting, (b) weighting.

same for all channels in the HC. Due to the varying tower size in the EC the parameter η_E is varying. The numerical values given below correspond to the small pads in the longitudinal section 5 of the EC and are scaled proportionally to $1/V$ for other towers, where V is the tower volume.

To compensate for the numerical reduction of the energies due to the weighting, the total energy of a shower is rescaled finally using

$$E^w = [\langle E_E\rangle/\langle E_E^w\rangle]E_E^w + [\langle E_H\rangle/\langle E_H^w\rangle]E_H^w,$$

where $\langle E_E\rangle$ and $\langle E_H\rangle$ are the average measured energies for pions of a given beam energy for the EC and the HC respectively (calibrated according to section 3.3.3), whereas $\langle E_E^w\rangle$ and $\langle E_H^w\rangle$ are the corresponding average weighted energies.

The parameters have been determined separately for each beam energy by the conditions

(1) $\langle E^w\rangle = E_{beam}$,
(2) the width of the energy distribution is minimum,
(3) electrons and pions of the same energy have the same response.

The parameters η_E and η_H turn out to be strongly correlated to C_E^{min} and C_H^{min} respectively. The latter can be fixed to $C_E^{min} = C_H^{min} = 0.68$ for all energies without significant loss of resolution.

To simulate realistic calorimeter measurements, it is important not to make any use of the knowledge of the beam energy in the analysis of individual events. Therefore, the energy dependence of the quantities η_E, η_H and $[\langle E_E\rangle/\langle E_E^w\rangle]$, $[\langle E_H\rangle/\langle E_H^w\rangle]$ and of the calibration constants c_E, c_H (see section 3.3.3) has been parametrized in a simple first approach by a linear dependence as shown in fig. 19. The energy of individual events has been obtained in the following way: First the true energy is estimated from the energy sum without weighting using $c_E = 3.11$ GeV/pC and $c_H = 4.30$ GeV/pC as determined at a beam energy of 50 GeV. (This estimated energy is already quite close to the corrected energy, for example, the average deviation is 4% for the pion data at 170 GeV.) Then, the parameters at the estimated energy as obtained by the parametrization shown in fig. 19 are used to compute the corrected energy as described above.

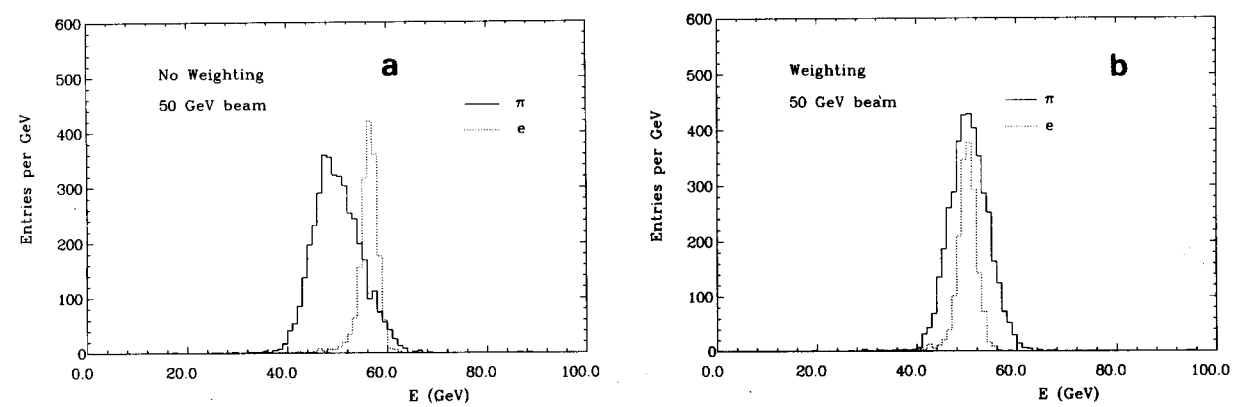

Fig. 18. Energy distribution for pions and electrons of 50 GeV: (a) no weighting, (b) weighting.

With this π^0 weighting technique the dependence of the energy E^w on the shower shape is considerably reduced as shown in figs. 16 and 17. It is also evident from fig. 18 that the ratio e/π is effectively 1. The resulting energy distributions are shown in fig. 14, and the widths of fitted Gaussian distributions are given in table 7 and fig. 15. The energy resolution is substantially improved using the weighting method. The ob-

Table 7
Energy resolution with π^0 weighting and contribution due to sampling fluctuations

E [GeV]	30	50	170	230
σ/E	0.089	0.071	0.042	0.036
$\sigma/\sqrt{E}$ [$\sqrt{\text{GeV}}$]	0.49	0.52	0.55	0.55
$S/\sqrt{E}$ [$\sqrt{\text{GeV}}$]	0.27	0.24	0.24	0.22

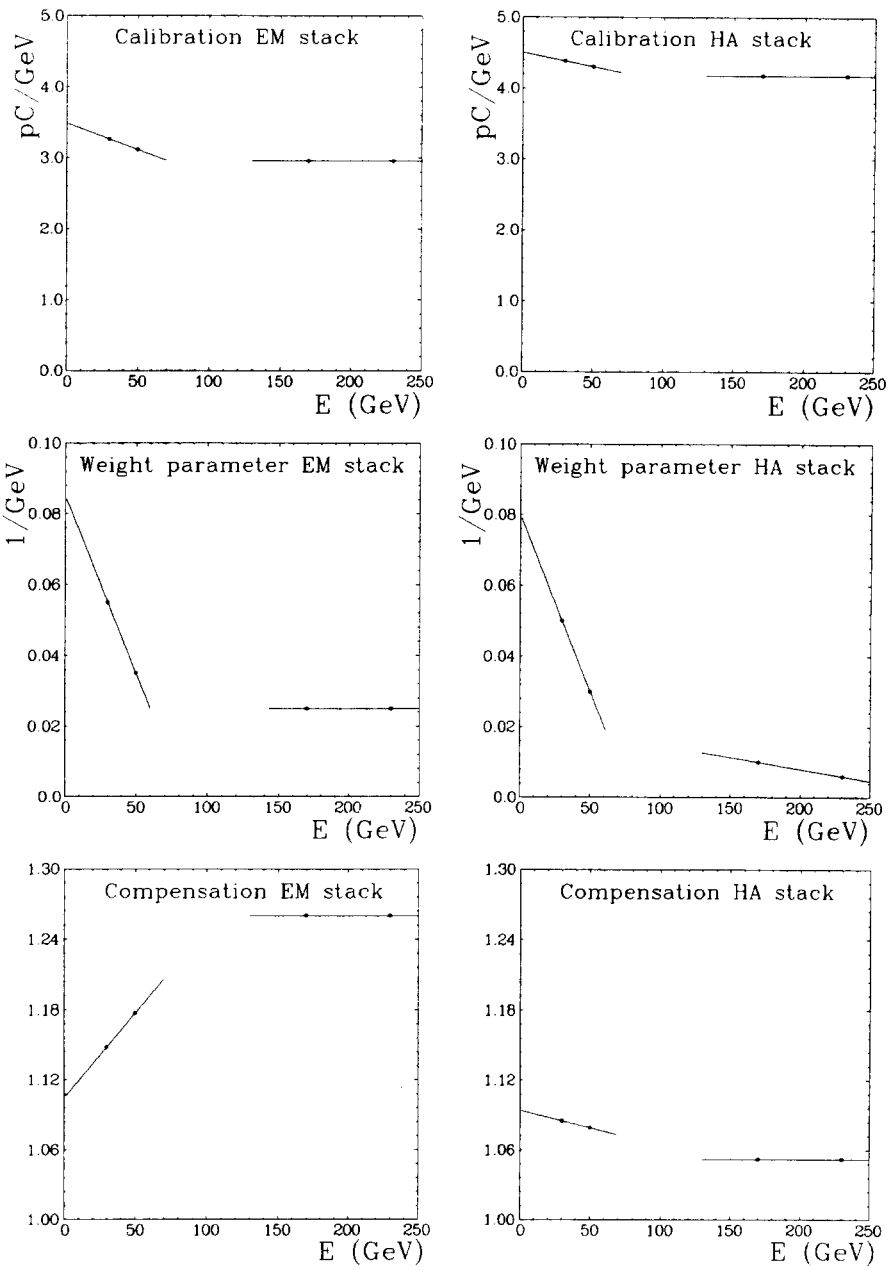

Fig. 19. Parametrization of c_E, c_H, and η_E, η_H and $\langle E_E\rangle/\langle E_E^w\rangle$, $\langle E_H\rangle/\langle E_H^w\rangle$ as a function of energy. The points show the beam energies used.

tained mean energy deviates from the beam energy by less than 1% in all cases for both electron and hadron initiated showers. A fit to the resolutions of the form

$$\sigma/E = \sqrt{A^2/E + B^2}$$

yields $A = 50.4\% \pm 0.4\%$, $B = 1.6\% \pm 0.1\%$.

A somewhat different weighting technique has been tried for the data of setup A. For the dependence of the energy on the deposited charge in the electromagnetic and hadronic calorimeter sections as third order polynomial has been assumed:

$$E_{\mathrm{em}} = \sum_{\mathrm{EC}} \left(C_1^{\mathrm{em}} Q_i + C_2^{\mathrm{em}} Q_i^2 + C_3^{\mathrm{em}} Q_i^3 \right),$$

$$E_{\mathrm{had}} = \sum_{\mathrm{HC}} \left(C_1^{\mathrm{had}} Q_i + C_2^{\mathrm{had}} Q_i^2 + C_3^{\mathrm{had}} Q_i^3 \right).$$

Based on the same number of free parameters, this is an approximation of the method above, but using a smooth function rather than fixed cutoff parameters $C^{\min}$. The parameters C_1 to C_3 for the electromagnetic and hadronic sections have been uniquely defined from a fit to the energy distribution of pions of a given energy. In the fit the energy resolution is minimized, while the pion energy is constrained to the nominal beam energy. The parameters obtained for the electromagnetic section show a rather modest energy dependence. The energy dependence of the corresponding parameters for the hadronic section is somewhat more pronounced, reflecting the energy dependence of the electromagnetic fraction of the deposited pion energy. Fig. 15 and table 8 show the energy resolution σ/E obtained for the data at 30, 80, 170 and 230 GeV. A fit to a function

$$\sigma/E = \sqrt{A^2/E + B^2}$$

yields $A = 44.9\% \pm 1.6\%$ and $B = 2.6\% \pm 0.2\%$.

3.3.5. Sampling fluctuations

The contribution of sampling fluctuations to the the resolutions can be evaluated due to the independent readout of x and y strips in the HC (see section 2.3.2.). Reading the x or y strips only corresponds to Cu absorber plates of 1 cm thickness. Assuming that the resolution for readout of x and y strips is given by

$$\sigma^2 = I^2 + S^2,$$

and for readout of x or y strips only by

$$(\sigma')^2 = I^2 + 2S^2,$$

Table 8
Energy resolution for pions using the π^0-weighting method II (data of setup A)

E_π [GeV]	30	80	170	230
σ/E	0.099	0.055	0.043	0.041
$\sigma/\sqrt{E}$	0.54	0.49	0.56	0.063

where S represents the sampling fluctuations and I the intrinsic resolution, the sampling fluctuations for 5 mm Cu can be determined and are given in table 7. The sampling terms obtained without π^0 weighting are very similar.

3.3.6. Jet energy resolution

As a special case we studied a subsample of early interactions in the calorimeter which is a somewhat better approximation to HERA jets as just single pions which often punch through the EC. With the requirement of an energy deposit of more than 0.4 GeV in the second longitudinal EC segment, we obtain events with the fraction $\langle E_{\mathrm{EC}} \rangle / E_{\mathrm{beam}}$ in the range 0.54 (230 GeV) to 0.65 (30 GeV) which might be reasonable for jets. The maximum deviation of the mean measured energy for this subsample from that of the whole sample is 1% (at 50 GeV). The resolutions are in the range $0.47/\sqrt{E}$ to $0.50/\sqrt{E}$. Further studies on jet reconstruction will be presented in a forthcoming paper [5].

4. Conclusions

A systematic study of a LAr calorimeter using lead (copper) in the e.m. (hadronic) section as absorber material has been performed for electrons and pions in the energy range from 10 to 230 GeV. For electrons an energy resolution of about $10\%/\sqrt{E}$ has been obtained, for pions the corresponding values range from $61\%/\sqrt{E}$ to $76\%/\sqrt{E}$. Even though the e/π ratio is not equal to unity, it has been shown that by applying the π^0-weighting technique the response to pions and electrons can be equalized. Exploiting this technique, an energy resolution of about $50\%/\sqrt{E}$ has been obtained for pions.

Acknowledgements

We would like to thank all our technical collaborators for their help and their contributions to the successful test of this calorimeter. In particular, we wish to thank G. Falley, J. Koll, and K. Thiele from DESY, C. Billat from Ecole Polytechnique, John O'Connor, T. Paris, and T. Roberts from the University of Houston, H. Laskus, H. Brettel, W. Pimpl, and P. Weissbach from MPI, Munich, and G. Bertalmio, J. Bossard, and J. Tichit from Saclay. We would also like to thank the staff at CERN for the operation of the SPS accelerator and the H6 beam line.

References

[1] Technical Proposal for the H1 Detector (March 1986).
[2] H1 Internal Report H1-05/85-19 (1985).

[3] CDHS collaboration, Nucl. Instr. and Meth. 180 (1981) 429.
[4] WA78 collaboration, Nucl. Instr. and Meth. A243 (1986) 348.
[5] H1 Collaboration, Detailed Calorimeter Test Results, in preparation.
[6] H6 beam tuning, CERN/SPS/EPB/PC (1981).
[7] H.W. Atherton et al., CERN/SPS/85-43 (1985).
[8] P. Coet, CERN/SPS 85-14 (1985).
[9] C. Bovet et al., CERN/SPS/82-13 (1982).
[10] H1 Collaboration, Results from the gaseous tail catcher, in preparation.
[11] E. Barrelet, P. Marbot and P. Matricon, Proc. Real Time Data Handling and Process Control, The Netherlands (1980).
[12] R.L. Ford and W.R. Nelson, SLAC-Report 210 (1978).
[13] R. Brun et al., CERN DD/EE/84-1 (1986).